



Fatigue damage development in 10CrMo9-10 steel for power plant pipes in as-received state and after 280,000 h of exploitation

Mateusz Kopec^{1,2} · Adam Brodecki¹ · Zbigniew L. Kowalewski¹

Received: 29 December 2022 / Revised: 13 February 2023 / Accepted: 12 March 2023
© The Author(s) 2023

Abstract

This paper discusses an effect of 280,000 h of exploitation under internal pressure of 2.9 MPa and high temperature of 540 °C on the mechanical properties of 10CrMo9-10 (10H2M) power engineering steel. The mechanical response of the specimens obtained from two pipes: a new in the as-received state and exploited for a long period was assessed through the uniaxial tensile tests and subsequent fatigue tests. The long-term, high-temperature exposure of 10H2M steel resulted in the deterioration of its mechanical properties and was quantitatively described as a function of the fatigue damage measure, φ , and the fatigue damage parameter D . Finally, the proposed methodology of power exponent approximation with both damage sensitive parameters (φ , D) enabled for successful determination of the 10H2M steel fatigue life.

Keywords Fatigue · Damage development · 10H2M steel · High-temperature aging

1 Introduction

With an increasing demand of the power plant industry, the operating parameters of working elements increased significantly in comparison to those used in the past. The aggressive conditions including the high temperature and internal pressure of the piping systems notably accelerate material degradation [1]. Such a situation requires continuous monitoring, which needs to be performed to maintain the required properties, and, as a consequence, further state exploitation and efficient estimation of the service life of working components [2]. Since the aggressive environment in which the power engineering components are working accelerates a development of damage dynamics significantly, it is extremely important to ensure the safety of power engineering steel pipes to minimize the operating costs of industrial structures and support a smooth workflow of power plants [3].

The good heat-resistant characteristics of chrome-manganese, perlitic creep-resistant structural steel (10H2M) are

decisive in essential reduction of the overall operating cost in steam-generating thermal power plants [4]. The long-term exposure to high temperature leads to its degradation, and finally to microstructural changes involving the transformation of the as-received fine-tempered martensitic laths into broader ferrite laths, and, moreover, into the equiaxed ferrite grain structure [5]. The transformed structure along with $M_{23}C_6/M_6C$ carbides (chromium, iron, molybdenum, and vanadium carbon compounds) concentrated on the ferrite grain boundaries affects effectively the mechanical response of 10H2M steel, including its fatigue response. Therefore, effective health monitoring of the elements made of power engineering steels through a series of destructive and non-destructive tests should be performed after a particular period of time [6]. To predict or determine the service life of components working under extreme conditions, comparative studies of the as-received and exploited materials are commonly employed. They could be effectively used to assess the actual mechanical response of materials subjected to long-term operations [7]. Furthermore, such comparative studies clearly indicate whether the exploited material could be further used without a decrease of safety and reliability of the power engineering constructions. Gwozdzik et al. [8] applied optical and transmission electron microscopy as well as standard tensile tests and Charpy tests on 10CrMo9-10 and 13CrMo4-5 steels (low-carbon chrome-molybdenum grade) before and after long-term operation at elevated

✉ Mateusz Kopec
mkopec@ippt.pan.pl

¹ Institute of Fundamental Technological Research Polish Academy of Sciences, 5b Pawińskiego Str., 02-106 Warsaw, Poland

² Imperial College London, London, UK

temperatures in a steam heater. Golasinski et al. [9] provided a detailed description of the microstructural changes in the high-chromium martensitic steels that occurred under creep conditions to further extend their time of safe operation in the particular structural elements of power systems. A similar approach was proposed by Singh et al. [10] who performed extensive creep testing of 1Cr1Mo $\frac{1}{4}$ V (chromium–molybdenum–vanadium low alloy forging cast steel) in the as-received (normalized and tempered) and aged conditions followed by scanning and transmission electron microscope observations to reveal the damage mechanisms and estimate the remaining service life. Dzioba et al. [11] used the true stress–true strain diagrams for an assessment of the in-service degradation of gas pipeline steels. The results demonstrated the advantage of such methodology in comparison to the stress–strain curves.

It should be highlighted that all these approaches are usually proposing a relatively simple set of mechanical tests and microstructural observations performed on the as-received and post-operational specimens. Such methodology offers only limited knowledge on the mechanical behaviour of long-time operated materials, since the actual behaviour under complex environmental conditions is usually insufficiently investigated. Therefore, this research aims to assess and quantitatively describe the effect of 280 000 h operating conditions on the microstructure, strength characteristics, and dynamics of fatigue damage development of 10H2M steel described as a function of the fatigue damage measure, φ , and the fatigue damage parameter D .

2 Materials and methods

2.1 Characterization of material

The material was supplied in the form of two 1-m-long pipes. The first pipe was operated for 280,000 h at the internal pressure of 2.9 MPa under temperature equal to 540 °C. The second one was delivered as a pipeline in the as-received state (normalization at 910–960 °C and high tempering at 650–780 °C) [9]. The chemical composition tests performed on both materials enabled confirmation of the agreement with the Polish Standards (PN-75/H-84024) [12] as presented in Table 1.

Table 1 Chemical composition of specimens made of 10H2M steel before and after exploitation compared to that required by the Polish Standards

	C	Si	Mn	P	S	Cr	Mo	Ni	Fe
As-received state	0.14	0.33	0.70	0.02	0.02	0.91	0.33	0.25	Bal
280 000 h of exploitation	0.16	0.35	0.61	0.02	0.02	0.92	0.38	0.25	Bal
PN-75/H-84024 [12]	0.10–0.17	<0.35	0.4–0.7	<0.025	0.02	0.7–1.15	0.4–0.6	<0.3	Bal

2.2 Experimental details

The hourglass specimens were extracted (wire-cut and machined) from two types of 10H2M steel pipelines as presented in Fig. 1a. Three specimens per condition were used to guarantee the reliability of the results obtained. The geometry of specimens for both standard tensile and fatigue tests is shown in Fig. 1b. They were machined in a computer numerical control (CNC) lathe machine using the same programme to ensure a surface finish and repeatability of the subsequent tests. A total number of 60 specimens were machined from two pipelines (30 specimens from each). Uniaxial tensile tests were performed at a strain rate equal to $2 \times 10^{-4} \text{ s}^{-1}$. The range of fatigue loads was established on the basis of yield strength $R_{0.2}$ determined from the uniaxial tensile test. The fatigue tests were performed in the range of stress amplitude from $\pm 250 \text{ MPa}$ to $\pm 400 \text{ MPa}$ using the MTS 858 testing machine, as shown in Fig. 1c. The fatigue tests were force controlled with zero mean value and constant stress amplitude with a frequency of 20 Hz. During the entire loading process, an MTS extensometer was used to monitor a diameter change in the specimen gauge length. The axial strain was calculated on the basis of transversal strain and Poisson's ratio. The fracture surface observation was performed using a JEOL field emission gun scanning electron microscope (SEM) operated at 20 kV. The qualitative chemical composition analysis was performed using Quanta 3D FEG field emission scanning electron microscope (SEM) operated at 20 kV with EDS detector.

3 Results and discussion

3.1 Mechanical testing of 10H2M steel

The representative strength characteristics of 10H2M steel in the as-received state and after the operation are shown in Fig. 2a. The reliability of the tensile test results was confirmed by testing five specimens accordingly. The average values of parameters determined from these tests are presented in Table 2. Interestingly, the results of tensile tests exhibited a significant decrease in yield point of about 86 MPa for the steel subjected to long-term operation. However, the ultimate tensile strength and ductility remained at a similar level. Nevertheless, both these parameters were still

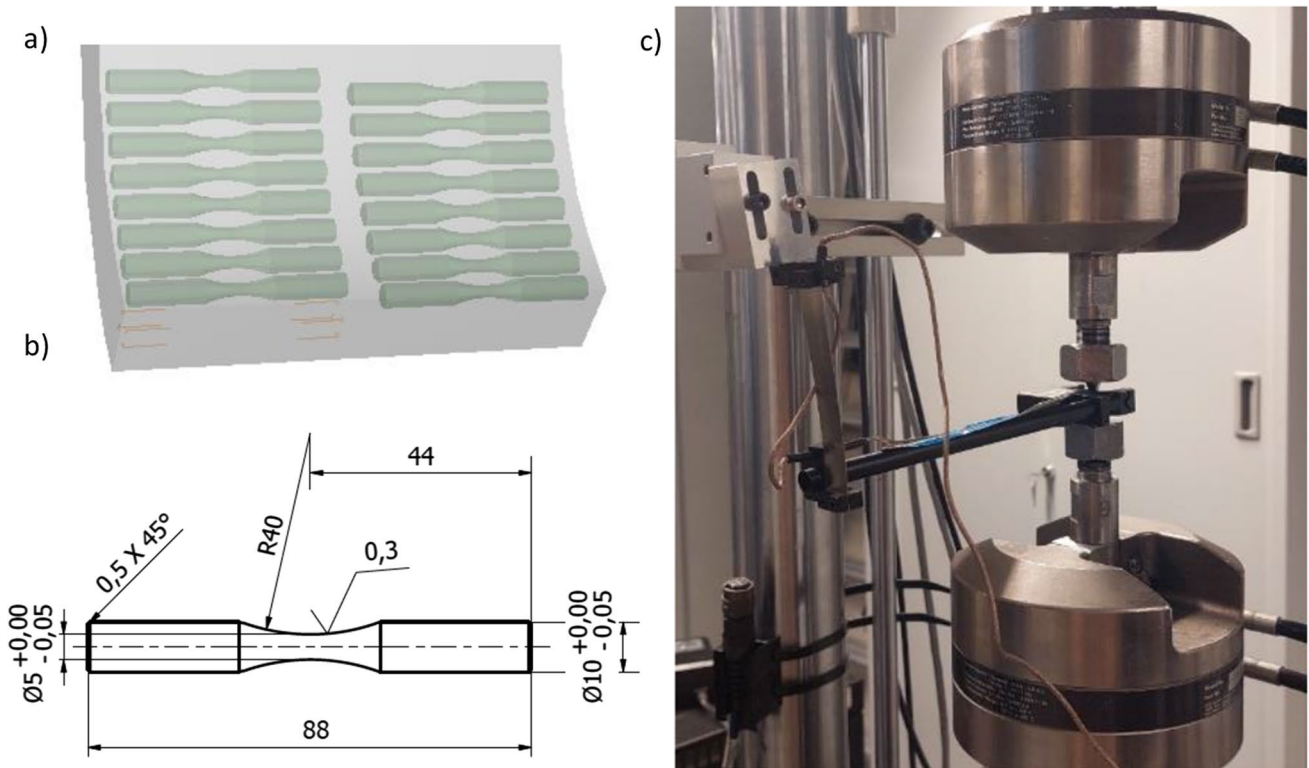


Fig. 1 Specimens' distribution in a pipe section (a), engineering drawing of the specimen (b), and general view of the experimental setup (c)

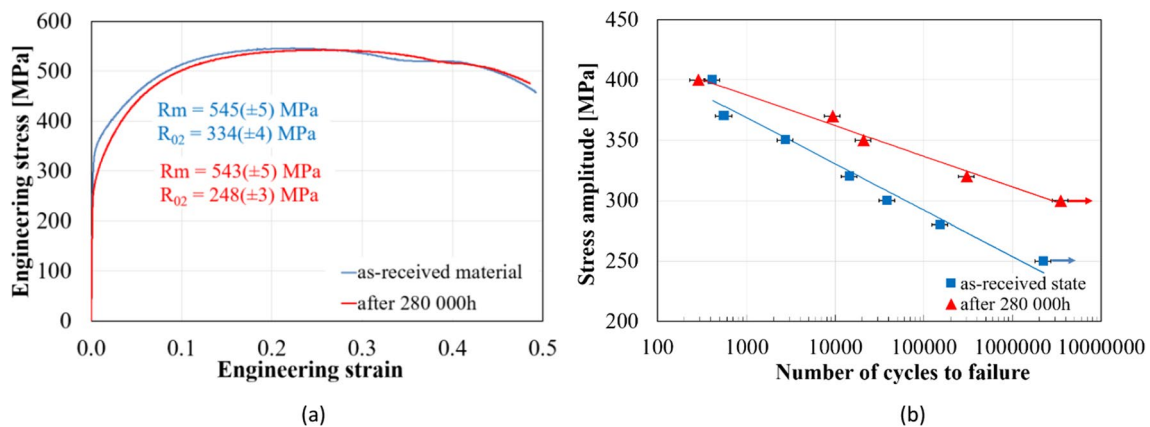


Fig. 2 Representative tensile curves for 10H2M steel in the as-received state and after exploitation (a); S–N curves for the steel in the as-received state and after exploitation (b)

Table 2 Mechanical parameters of 10H2M steel before and after exploitation compared to those of the Polish Standards

	R_m [MPa]	$R_{0,2}$ [MPa]	A [%]
As-received state	545(±5)	334(±4)	48%(±1)
280 000 h of exploitation	543(±5)	248(±3)	46%(±1)
PN-75/H-84024 [12]	> 415	> 205	> 30%

R_m tensile strength, $R_{0,2}$ yield point, A elongation

within a range of PN-75/H-84024 standards [12] for both types of specimens.

Subsequent comparative fatigue tests performed to elaborate the S–N curves for both states of the steel in question revealed that due to exploitation, a significant decrease of fatigue lifetime was observed for the entire range of stress amplitudes considered. One should highlight a considerable drop of the number of cycles to failure for the exploited steel

in comparison to the same material tested in the as-received state under the same stress amplitude (Fig. 2b). Such tendency can be observed for majority of stress amplitude magnitudes taken into account.

3.2 Microstructural analysis of damage development

The high-temperature, time-intensive exploitation for 280,000 h at 540 °C and the internal pressure of 2.9 MPa led to the significant degradation of the 10H2M steel microstructure, as shown in Fig. 3. The microstructure of 10H2M steel in the as-received (normalized and tempered) state consisted of the typical ferritic–bainitic microstructure [11] in which packets of lath or plate-shaped ferrite, associated with carbide particles, could be observed (Fig. 3a–b). On the other hand, the exploited material was characterized by degraded bainite, a small amount of ferrite and precipitated carbides concentrated at the grain boundaries [8] (Fig. 3c–d).

After fatigue tests, a fracture analysis was performed. Characteristic fracture surface morphologies observed for almost all steel specimens included: crack initiation area surrounded by radial streaks along the crack propagation

direction and a relatively flat surface (marked as I in Fig. 4), propagation area with microvoids and dimples (marked as II in Fig. 4), and instantaneous fracture area (marked as III) [13]. The crack initiation areas were mainly found at the edge of the specimen so in the areas, where the stress concentration occurs due to sub-surface defects or non-metallic inclusions [14]. The propagation area characterized by microvoids consisted also the secondary cracks, which were formed due to connecting pores. Subsequent cleavage steps parallel to the direction of crack propagation form the so-called “river patterns” [13]. On the other hand, the ductile fracture surface of a greater contribution of the fine morphological cavities in the form of craters and non-metallic inclusions was observed for the as-received material after testing at stress amplitude of 400 MPa.

It was reported that the long-term operation of power engineering steels leads to significant changes in their microstructure which mainly include the diffusion of alloying elements out of the bainite, formation and coagulation of carbide precipitates at the grain boundaries, and partial transformation of original bainite to ferrite [8, 15]. It was

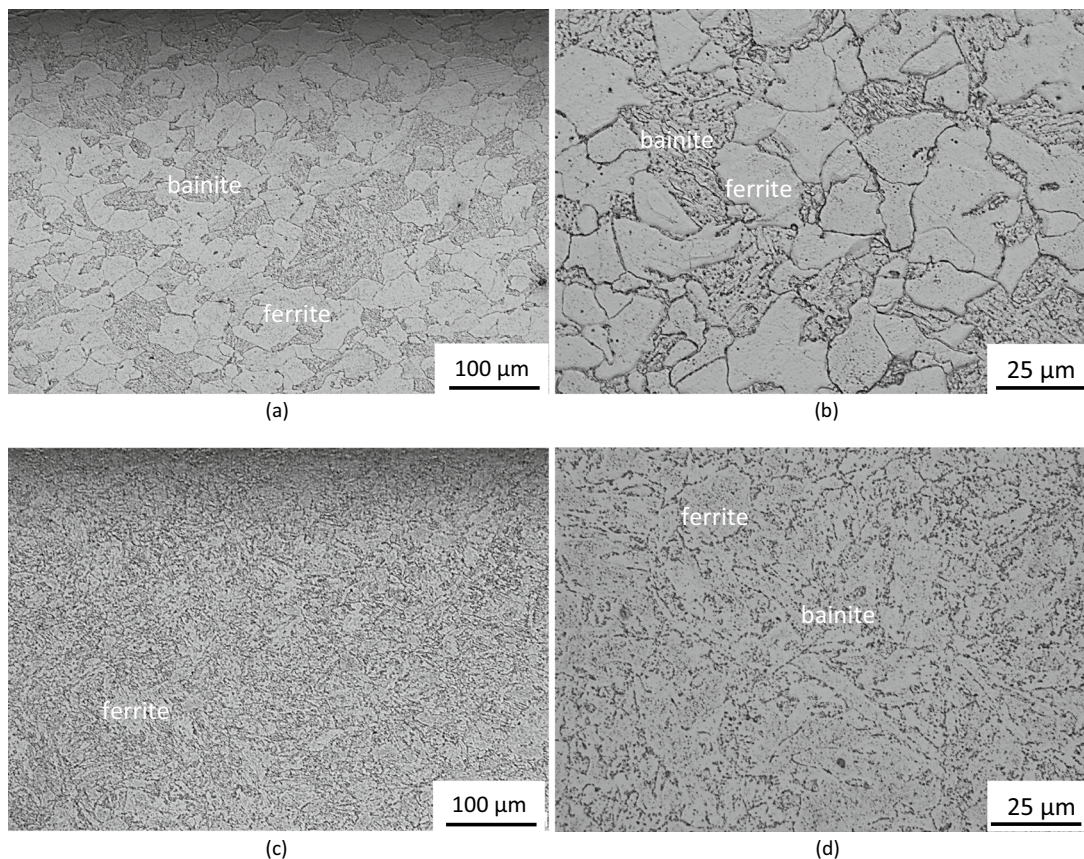


Fig. 3 Microstructure of 10H2M steel in the as-received state (a–b) and after exploitation (c–d)

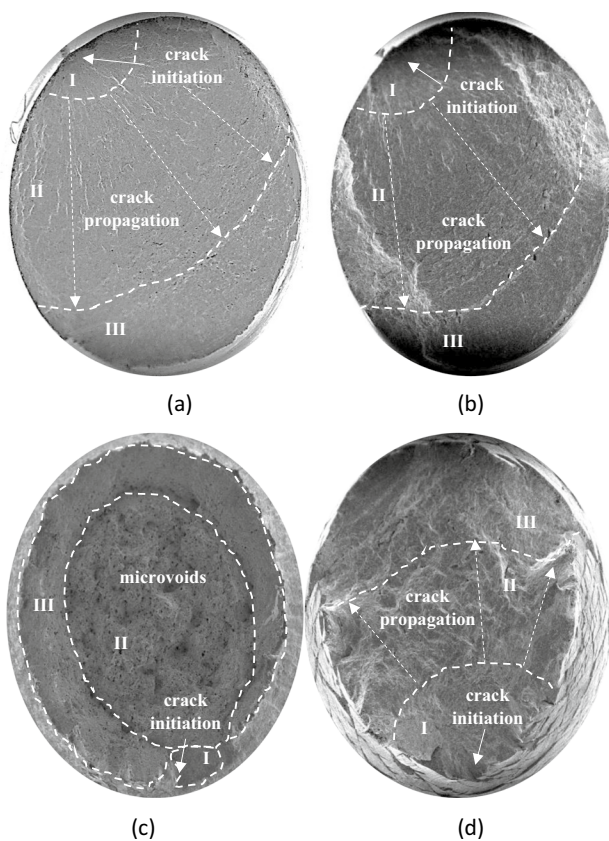


Fig. 4 Fracture surface of the as-received (a) and exploited (b) specimen after testing at the stress amplitude of ± 320 MPa; the fracture surface of the as-received (c) and exploited (d) specimen after testing at the stress amplitude of ± 400 MPa

confirmed that such processes are directly responsible for the reduction of the strength parameters of the steel [15].

3.3 Quantitative assessment of the fatigue damage development in 10H2M steel

The quantitative assessment of the fatigue damage development was performed based on the mechanical response of 10H2M steel registered in successive cycles for all levels of constant stress amplitude. The representative graphs were presented for the as-received and exploited material subjected to limit stress amplitudes between ± 320 MPa and ± 400 MPa to reveal both the effect of stress amplitude and the state of development of damage mechanism in the steel tested (Fig. 5).

The analysis including the monitoring of hysteresis loop changes in the subsequent cycles enabled an identification of two main mechanisms responsible for fatigue damage development: ratcheting and cyclic plasticity [16]. It can be easily noticed that ratcheting is characterized by negligible small changes in the hysteresis loop width together with simultaneous increase of the mean level of

strain in subsequent cycles, while for the cyclic plasticity, considerable changes of the hysteresis loop width are observed [17]. Similarly to X10CrMoVNb9-1 (high-temperature resistant, martensitic high-chromium–molybdenum–alloyed power engineering steel) [7], 10H2M steel exhibited a combination of both mechanisms (Fig. 5). It should be emphasised, however, that for the as-received material subjected to the stress amplitude of ± 320 MPa, ratcheting is the dominating mechanism, since the width of hysteresis loop changes slightly up to 200,000 cycles (Fig. 5a). On the other hand, a considerable change in the width was observed for the exploited steel. The 19th loop registered for that state was significantly wider than the 200,000th one for the as-received material (Fig. 5b). Similar behaviour was observed for both states of steel subjected to fatigue loading at the stress amplitude of 400 MPa. The combination of ratcheting and cyclic plasticity mechanisms led to the increase of the hysteresis loop width and its simultaneous shift (Fig. 5c–d).

It should be mentioned that the 10H2M steel was subjected to fatigue testing slightly above the yield stress level, and thus, the high plastic deformation was induced at the initial cycles. Therefore, the analysis of fatigue response was treated in terms of strain versus time (Fig. 6) and number of cycles to failure (Fig. 8). It is easy to notice that the material subjected to fatigue at the same stress amplitude was characterized by a different strain response which was dependent on its state. The strain response of the exploited material subjected to fatigue at both stress amplitudes considered (320 MPa and 400 MPa) was found as two times higher than that for the as-received state obtained. Interestingly, the effect of long-time exploitation was more prominent under a higher stress amplitude, i.e., 400 MPa, under which the strain signal registered for the material subjected to 280,000 h of work was 220% higher than that for the as-received one.

The comparison of mechanical responses registered for both states of steel and presented in the form of S–N curve represents the conventional approach, that could be effectively used to assess an effect of long-time exploitation on the material integrity. It should be mentioned, however, that determination of the typical S–N curve is quite costly and time-consuming [18]. An alternative method presented by authors [7] is based on the evolution of deformation dynamic development due to the ratcheting and cyclic plasticity registered in subsequent cycles for the range of stress amplitudes applied (Fig. 7). These changes were further parametrized and described as the fatigue damage measure, ϕ , and fatigue damage parameter D. Since the microstructural changes that occurred during cyclic degradation may be attributed to particular changes in the stress–strain response, effective indicators were used to describe and quantify each deformation mechanism found in subsequent cycles:

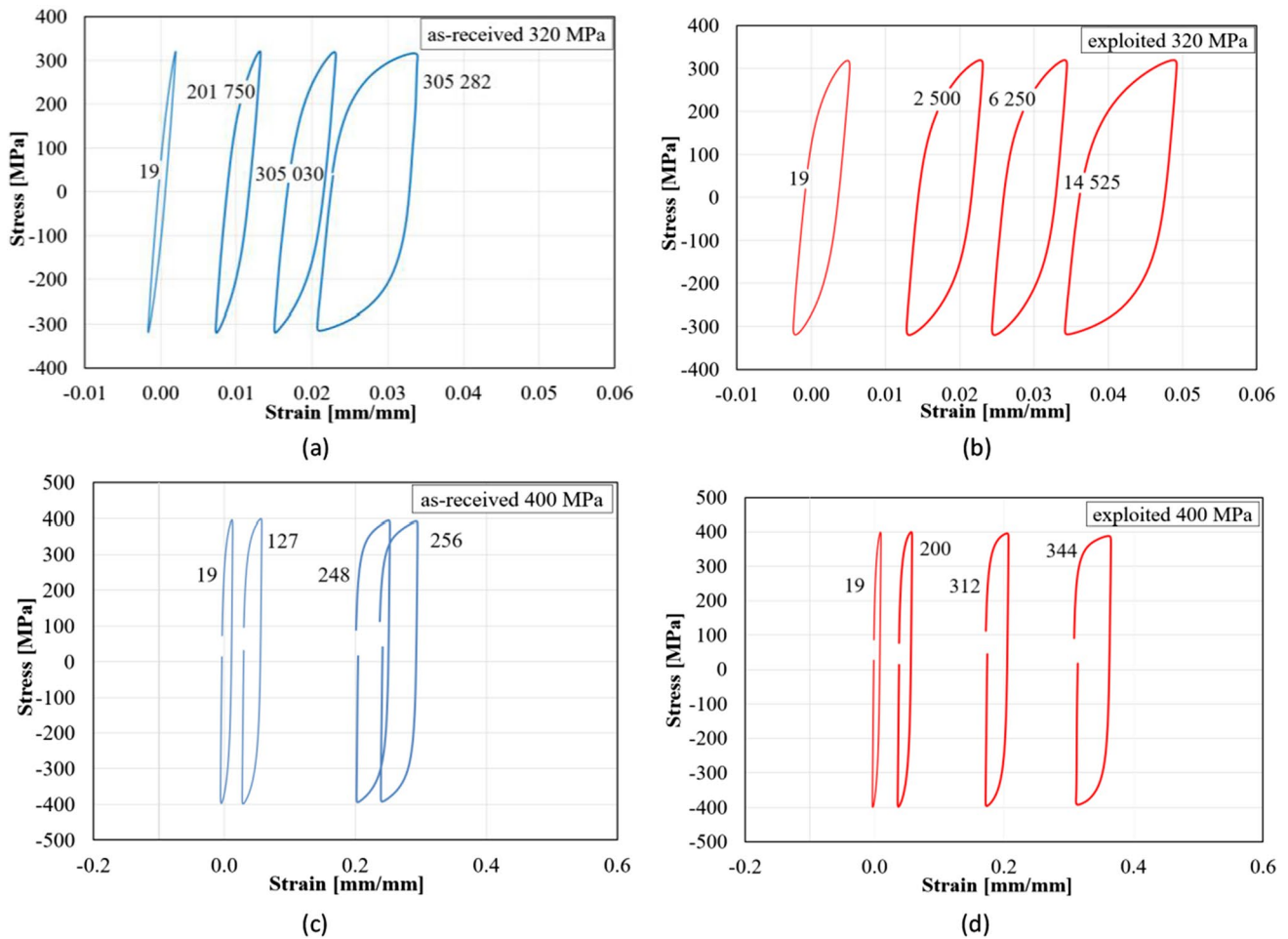


Fig. 5 Fatigue development in the selected cycles for the steel in the as-received state (a, c); steel after exploitation for 280 000 h (b, d) at the amplitude of ± 320 MPa and ± 400 MPa

- ratcheting generated by local deformation around the voids, inclusions, and other defects; the process was related to the mean inelastic strain describing a shift of the hysteresis loop under unloaded state;
- cyclic plasticity generated by dislocation movement at the level of local grains and slip bands; the mechanism was related to the hysteresis loop width changes at the total unloading of the material.

Since both mechanisms were observed for 10H2M steel, their combination was responsible for damage development. To reflect such type of damage the following damage measure was proposed:

$$\varphi = \varepsilon_w + \varepsilon_m, \tag{1}$$

where ε_w is inelastic strain amplitude being damage indicator that characterizes a width of the hysteresis loop at total

unloading, and ε_m is mean inelastic strain responsible for a shift of the hysteresis loop under unloaded state.

The inelastic strain amplitude was measured at the total unloading of the material. It can be described in a single cycle by the simple expression in the following form:

$$\varepsilon_w = \frac{\varepsilon_{min}^{F=0} - \varepsilon_{max}^{F=0}}{2}. \tag{2}$$

The mean inelastic strain was also captured under the unloaded state. It can be defined by the following relationship:

$$\varepsilon_m = \frac{\varepsilon_{min}^{F=0} + \varepsilon_{max}^{F=0}}{2}. \tag{3}$$

Changes in the fatigue damage measure, φ , were used to determine evolution of the damage parameter D. The

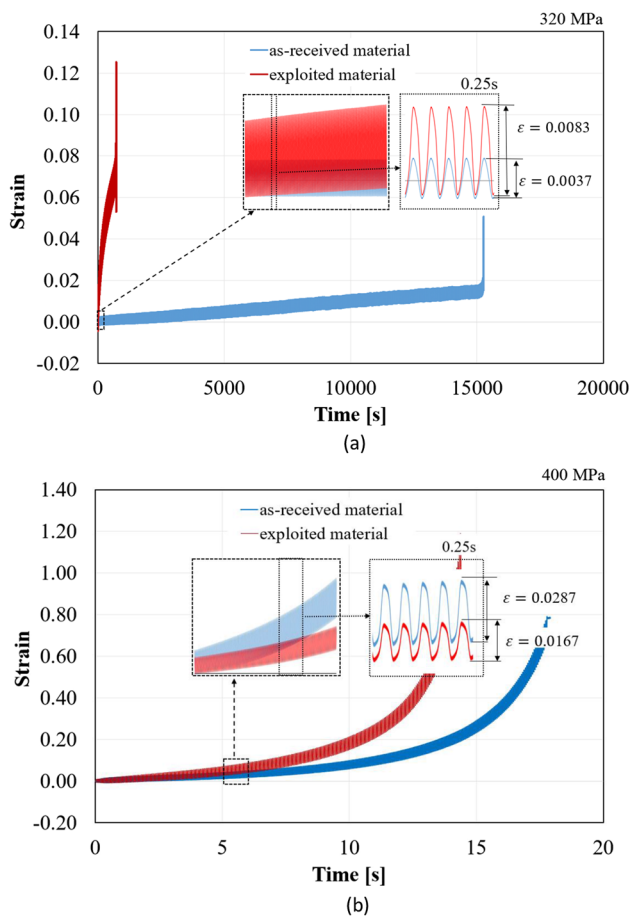


Fig. 6 Strain–time characteristics evolution of the 10H2M steel specimens subjected to the stress amplitude of ± 320 MPa (a) and ± 400 MPa (b)

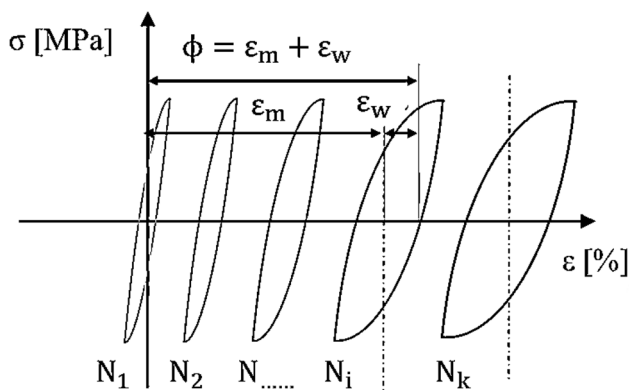


Fig. 7 Hysteresis loop evolution in subsequent fatigue cycles for 10H2M steel in both (as-received and exploited) conditions

fatigue damage parameter D describes the dynamics of deformation changes in subsequent cycles. It is defined by the relationship

$$D = \frac{\varphi_N - \varphi_{min}}{\varphi_{max} - \varphi_{min}}, \tag{4}$$

where φ_N is current value of the fatigue damage development measure in the cycle N , φ_{min} is minimum value of the fatigue damage development measure at the beginning of the cyclic loading, i.e., for the cycle $N=1$, and φ_{max} is maximum value of the fatigue damage development measure for the last cycle representing of the stable damage development N_f .

The accelerated dynamics of fatigue damage development could be clearly observed for the exploited steel by comparing an evolution of the fatigue damage measure and fatigue damage parameter as a function of the number of cycles to failure (Fig. 8). Both states of 10H2M steel exhibited significantly different dynamics, since the damage of exploited steel occurred much earlier than in the case of as-received material. Based on the fatigue damage measure (Fig. 8a, c), it could be demonstrated that the exploited steel was characterized by notably greater dynamics of damage development, since the growth of φ parameter observed up to 10 000 cycles indicates the simultaneous increase of hysteresis loop width. Such behaviour was not observed for the as-received material, which means that the ratcheting was the dominant deformation mechanism in this case. Such significant differences were not observed for the stress amplitude of ± 400 MPa (Fig. 8b, d); however, the damage dynamics for exploited material were still more pronounced.

One could find that the character of curve slope is more steady for the as-received material and the degradation rate is permanently growing from near zero values reflecting its undeformed state. On the other hand, the exploited material just at the beginning of deformation exhibits higher values of both fatigue damage measure and fatigue damage parameter. Such characteristic feature well corresponds to its changed internal state.

3.4 Determination of the fatigue stress amplitude limit based on the degradation development of 10H2M steel

Finally, the determination of fatigue stress amplitude limit was performed by approximation of exponential curves obtained by fatigue damage measure, φ , and fatigue damage parameter D correlation for each stress amplitude (Fig. 9). First, Eqs. 1 and 4 were used to determine both parameters φ and D for each stress amplitude. The evolution of these parameters in individual cycles enabled for approximation of these exponential curves. Subsequently, the exponent values of functions describing each curve were compared on the graph as a function of stress amplitude values for both states of the material tested. Finally, a linear trend line was used to predict the fatigue stress amplitude limit. Such limit, according to the Polish Standards [19], represents stress amplitude

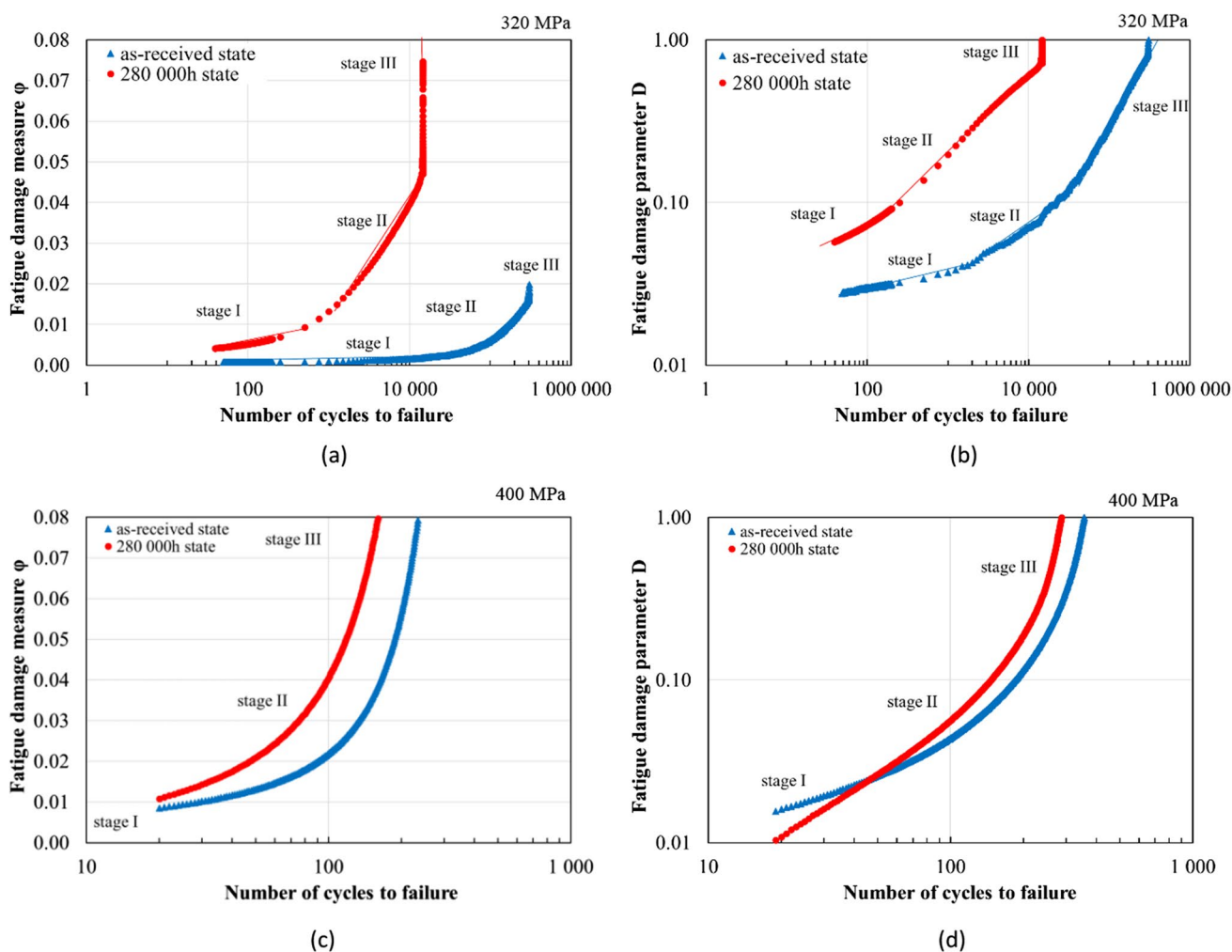


Fig. 8 Development of the fatigue damage for stress amplitude of ± 320 MPa and ± 400 MPa expressed by fatigue damage measure ϕ variations as a function of the number of cycles (a, c), and evolution of the fatigue damage parameter D (b, d)

that enables carrying out 10^7 loading cycles. In the method presented here, the fatigue stress amplitude limit value corresponds to the intersection point of the line representing an approximation of the experimental results with the x-axis. Such determined value was equal to 245 MPa for the steel exploited for 280,000 h, and 293 MPa for the material in the as-received state. One should highlight a good agreement between these results and those obtained from the S–N curves (250 MPa for the steel exploited for 280 000 h, 300 MPa for the material in the as-received state) (Fig. 9, Table 3).

Since the S–N curves represent the stress amplitude values as a function of the number of cycles to failure only, the fatigue damage dynamics that occurred during fatigue testing could not be assessed effectively. It was confirmed that the methodology presented enables successful determination of the fatigue stress amplitude limit along with the identification of fatigue damage mechanisms [7]. In this paper, the

effect of long-term exploitation for 280,000 h on the fatigue response of 10H2M steel was successfully performed using the approximation of the exponent values obtained from the very first to the last loading cycle. It was found that fatigue damage measure and fatigue damage parameters related to the hysteresis loop width and its shift could be used to identify the physical mechanisms of damage evolution that occurred during fatigue testing.

4 Conclusions

In this paper, fatigue damage development in 10H2M steel for power plant pipes in the as-received state and after 280,000 h of exploitation was described and analysed using the conventional S–N curves and power exponent approximation method of fatigue damage measure ϕ and fatigue damage parameter D. The long-term exploitation led to the

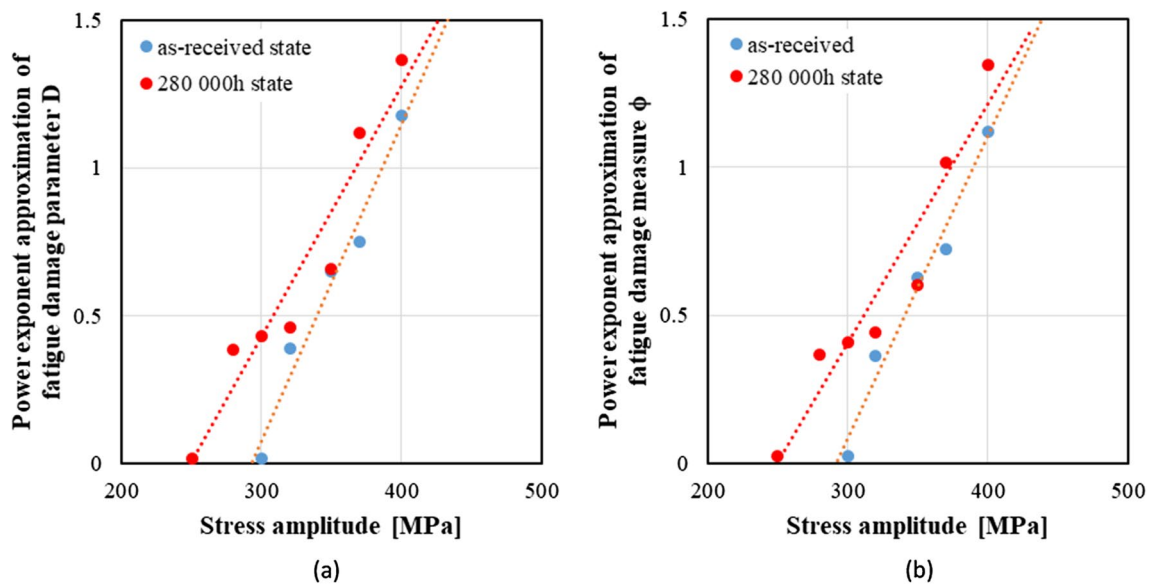


Fig. 9 Determination of the cyclic stress amplitude limit on the basis of power exponent approximation in the case of fatigue damage measure φ (a) and fatigue damage parameter D (b)

Table 3 Fatigue stress amplitude limit values determined using the S–N curve and approximation of exponential curves obtained by fatigue damage measure, φ , and fatigue damage parameter D approach

	S–N [MPa]	Approximation of exponential curves [MPa]
As-received	300	293
280 000 h of exploitation	250	245

significant reduction of service life of the steel in question captured for the same stress amplitudes, which was directly attributed to the microstructural changes occurred during operation. The initial ferritic–bainitic microstructure with packets of lath or plate-shaped ferrite transformed into degraded bainite, a small amount of ferrite and precipitated carbides concentrated at the grain boundaries.

Finally, it can be concluded that the methodology proposed was found as an effective tool for predicting the fatigue stress amplitude limit and could be successfully used as an additional approach providing much more data characterizing fatigue damage development than S–N curves.

Acknowledgements The authors would like to express their gratitude to the technical staff—Mr M. Wyszowski and Mr A. Chojnacki for their kind help during the experimental part of this work.

Author contributions Conceptualization: MK and ZK; data curation: MK and AB; formal analysis: MK; investigation: AB and MK; methodology: AB, MK, and ZK; project administration: ZK; supervision:

MK and ZK; validation: MK and ZK; visualization: AB and MK; writing—original draft: MK and AB.; writing—review & editing: ZK.

Funding This work has been partially supported by the National Science Centre under Grant No. 2019/35/B/ST8/03151.

Data availability Data available on request from the authors.

Declarations

Conflict of interest The authors declare that they have no known competing financial interests or personal relationships that could have appeared to influence the work reported in this paper.

Ethical approval This article does not contain any studies with human participants or animals performed by any of the authors.

Open Access This article is licensed under a Creative Commons Attribution 4.0 International License, which permits use, sharing, adaptation, distribution and reproduction in any medium or format, as long as you give appropriate credit to the original author(s) and the source, provide a link to the Creative Commons licence, and indicate if changes were made. The images or other third party material in this article are included in the article’s Creative Commons licence, unless indicated otherwise in a credit line to the material. If material is not included in the article’s Creative Commons licence and your intended use is not permitted by statutory regulation or exceeds the permitted use, you will need to obtain permission directly from the copyright holder. To view a copy of this licence, visit <http://creativecommons.org/licenses/by/4.0/>.

References

- Dudziak T, Jura K, Dudek P. Sulphidation of low-alloyed steels used in power industry. *Oxid Met*. 2019;92:379–99. <https://doi.org/10.1007/s11085-019-09929-7>.
- Ma Q, Tian G, Zeng Y, Li R, Song H, Wang Z, Gao B, Zeng K. Pipeline in-line inspection method. *Instrumentation Data Manag Sens*. 2021;21:3862. <https://doi.org/10.3390/s21113862>.
- Dudziak T, Łukaszewicz M, Simms N. Analysis of high temperature steam oxidation of superheater steels used in coal fired boilers. *Oxid Met*. 2016;85:171–87. <https://doi.org/10.1007/s11085-015-9593-9>.
- Sirohi S, Kumar S, Bhanu V, et al. Study on the variation in mechanical properties along the dissimilar weldments of P22 and P91 steel. *J Mater Eng Perform*. 2022;31:2281–96. <https://doi.org/10.1007/s11665-021-06306-x>.
- Liu j, Hao XJ, Zhou L, Strangwood M, Davis CL, Peyton A.J., Measurement of microstructure changes in 9Cr–1Mo and 2.25Cr–1Mo steels using an electromagnetic sensor. *Scripta Materialia*, Vol. 66(6): p. 367–370, 2012. <https://doi.org/10.1016/j.scriptamat.2011.11.032>
- Kukla D, Kowalewski ZL, Grzywna P, Kubiak K, Assessment of fatigue damage development in power engineering steel by local strain analysis, *Kovove Materialy–Metallic Materials*, ISSN: 0023–432X, Vol.52, No.5, pp.269–277, 2014
- Kopec M, Kukla D, Brodecki A, Kowalewski ZL, Effect of high temperature exposure on the fatigue damage development of X10CrMoVNb9–1 steel for power plant pipes, *Int J Pressure Vessels Piping*, ISSN: 0308–0161, 189: 104282–1–16, 2021 <https://doi.org/10.1016/j.ijpvp.2020.104282>
- Gwoździk M, Motylenko M, Rafaja D, Microstructure changes responsible for the degradation of the 10CrMo9–10 and 13CrMo4–5 steels during long-term operation, *Materials Res Express*, 7, 2020, 016515 <https://doi.org/10.1088/2053-1591/ab5fc8>
- Golański G, Kolan C, Jasak J Degradation of the microstructure and mechanical properties of high-chromium steels used in the power industry. In: Tanski T, Sroka M, Zielinski A editors. *Creep*. London: IntechOpen; 2017 <https://doi.org/10.5772/intechopen.70552>
- Singh K, Kamaraj M. Microstructural degradation in power plant steels and life assessment of power plant components. *Procedia Engineering*. 2013;55:394–401. <https://doi.org/10.1016/j.proeng.2013.03.270>.
- Dzioba I, Zvirko O, Lipiec S, Assessment of Operational Degradation of Pipeline Steel Based on True Stress–Strain Diagrams. In: Bolzon G, Gabetta G, Nykyforchyn H (eds) *Degradation assessment and failure prevention of pipeline systems*. Lecture Notes in Civil Engineering, vol 102. Springer, Cham. 2021 https://doi.org/10.1007/978-3-030-58073-5_14
- Polish Standards PN-75/H-84024—Steels for elevated temperature service—Grades
- Pandey C, Saini N, Mohan Mahapatra M, Kumar P Study of the fracture surface morphology of impact and tensile tested cast and forged (C&F) Grade 91 steel at room temperature for different heat treatment regimes, *Eng Failure Anal*, 71, 2017, 131–147 <https://doi.org/10.1016/j.engfailanal.2016.06.012>
- Łuczak K, Wolany W. The influence of the parameters of heat treatment on the mechanical properties of welded joints. *Arch Mater Sci Eng*. 2019;95(2):55–66. <https://doi.org/10.5604/01.3001.0013.1731>.
- Golański G, Zielińska-Lipiec A, Zieliński, effect of long-term service on microstructure and mechanical properties of martensitic 9% Cr steel. *J Mater Eng Perform*. 2017;26:1101–7. <https://doi.org/10.1007/s11665-017-2556-3>.
- Spriestersbach D, Kerscher E. The role of local plasticity during very high cycle fatigue crack initiation in high-strength steels. *Int J Fatigue*. 2018;111:93–100. <https://doi.org/10.1016/j.ijfatigue.2018.02.008>.
- Pelleg J (2013) Fracture. In: *mechanical properties of materials. solid mechanics and its applications*, vol 190. Springer, Dordrecht. https://doi.org/10.1007/978-94-007-4342-7_7
- Kulkarni A, Dwivedi DK, Vasudevan M. Study of mechanism, microstructure and mechanical properties of activated flux TIG welded P91 Steel-P22 steel dissimilar metal joint. *Mater Sci Eng, A*. 2018;731:309–23. <https://doi.org/10.1016/j.msea.2018.06.054>.
- Polish Standards PN10216–2: 2004—Steel tubes for pressure purposes—Technical delivery conditions—Part 2: Non-alloy and alloy steel tubes with specified elevated temperature properties

Publisher's Note Springer Nature remains neutral with regard to jurisdictional claims in published maps and institutional affiliations.